# Applied Modeling of the Nighttime Surface Energy Balance over Land

A. A. M. HOLTSLAG

*Royal Netherlands Meteorological Institute, de Bilt, The Netherlands*

H. A. R. DE BRUIN

*Department of Physics and Meteorology, Agricultural University of Wageningen, The Netherlands*

(Manuscript received 25 April 1987, in final form 30 October 1987)

ABSTRACT

In this paper a semiempirical scheme is proposed which relates the nocturnal surface fluxes of sensible heat, latent heat, and momentum to routine weather data. The main components of the surface radiation and energy balance over land are described on a half-hourly basis. Observations over a grass-covered surface at Cabauw are used to investigate topics proposed in the literature, and to develop new parameterizations. The input data of the scheme are total cloud cover, wind speed, air temperature, and specific humidity deficit at single heights in the atmospheric surface layer. A semiempirical expression is proposed for the estimation of the soil heat flux. Also the relation between the surface radiation temperature and the temperature at the level of the roughness length is described semiempirically. It is found that their difference is considerable, especially for low wind speeds. The output of the scheme is presented in terms of the main forcing terms. On average, the agreement of the model quantities with observations is reasonable. For instance, for clear skies with total cloud cover $N \leqslant 0.25$, it appears that root mean square errors are at best 9 W m$^{-2}$ for sensible heat flux, 6 W m$^{-2}$ for latent heat flux, 9 W m$^{-2}$ for soil heat flux, 13 W m$^{-2}$ for net radiation, and 1.8 K for surface radiation temperature. The temperature profile up to 80 m is well described by the present scheme. The difference of the scheme with previous methods in literature is discussed.

## 1. Introduction

The turbulent state of the nocturnal atmospheric boundary layer (NABL) is primarily determined by the surface fluxes of sensible heat and momentum. In NABL models, which are needed, e.g., for air pollution studies and short term weather forecasts, the fluxes have to be parameterized in terms of routine weather data or in terms of output parameters of meteorological models.

It is the objective of this paper to present such a parameterization scheme for the surface fluxes of sensible heat, latent heat and momentum. For this, the complete surface radiation and surface energy budget are treated and parameterized. The scheme requires total cloud cover, and wind speed, air temperature and specific humidity deficit at single heights in the surface layer. The scheme can be regarded as the counterpart of the daytime scheme by Holtslag and Van Ulden (1983).

Venkatram (1980) proposed a very simple method for the evaluation of the surface flux of sensible heat. He showed that the turbulent temperature scale $\theta_*$ (for its definition see section 3) is more or less constant for clear sky conditions. Holtslag and Van Ulden (1982) generalized this approach and showed $\theta_*$ to be dependent on total cloud cover. Such a method appears to be suitable for the description of the nocturnal wind profile at Cabauw up to ~100 m (Holtslag 1984), and the turbulent height of the NABL (Nieuwstadt 1984b).

The drawback of Venkatram's approach and its variants, is that $\theta_*$ does not vanish at low wind speeds. The latter has to be expected for cases in which turbulence cannot be maintained, and is confirmed by observations (Van Ulden and Holtslag 1983). Moreover, Venkatram's approach does not describe the entire energy balance at the surface.

Recently, Van Ulden and Holtslag (1983, 1985) presented a more complete model for the nocturnal energy budget. They showed that $\theta_*$ is approximately constant, within a certain range of wind speed. Moreover, the constant is directly related to the "isothermal" net radiation (see section 3a), which is primarily determined by total cloud cover. Therefore, the model by Van Ulden and Holtslag can explain the empirical results of Venkatram (1980) and Holtslag and Van Ulden (1982).

The present study can be regarded as an extension of the work by Van Ulden and Holtslag (1983, 1985). For example, we modified their descriptions of soil heat flux and evaporation. Also the vertical water vapor transport within the soil layer is accounted for, which

*Corresponding author address:* Dr. A. A. M. Holtslag, Royal Netherlands Meteorological Inst., P.O. Box 201, 3730 AE de Bilt, The Netherlands.



© 1988 American Meteorological Society

may cause dew at the surface (e.g., Monteith 1963; Oke 1978). Moreover, use has been made of the work on flux-profile relations by Hicks (1976) and others, leading to a better description of the nocturnal temperature profile in very stable conditions. In addition, we take into account that the sinks or sources of momentum, heat and radiation are at (apparent) different levels near the surface (e.g., Garratt and Hicks 1973; Brutsaert 1982).

In the last decades many micrometeorological experiments have been carried out. Nevertheless, there are only a few reliable observations of the surface fluxes during nighttime. The main reason for this is the fact that the absolute magnitude of the fluxes are often small and of the same order as the instrumental errors. Moreover, not all the quantities of the surface energy budget are completely understood (section 3). This means that large scatter is to be expected when model predictions and observations are compared.

In this study we will make use of a fairly complete dataset collected at Cabauw (section 2). The set is used both for comparison and parameterization purposes. Therefore some of the proposed parameterizations need further verification at other sites. Nevertheless, we believe that the present methods will be useful for climatological studies, engineering design purposes, air pollution stability classification, etc.

Besides the different terms of the surface energy budget, the surface radiation temperature also is described by our model. The latter is defined as the temperature that determines the outgoing longwave radiation (see section 3b). As such, it is often used in remote sensing studies. Calculated values of this quantity are compared with direct observations of an infrared thermometer. Since, the entire temperature profile (inclusive the surface), is described by our approach, the model might be useful for agricultural studies as well (e.g., frost problems).

## 2. Dataset

In this study we analyze observations from the 200 m tower and the micrometeorological field at Cabauw, The Netherlands. A description of the Cabauw facilities can be found in Driedonks et al. (1978). The Cabauw datasets are described by Wessels (1984), and those collected at the micrometeorological field by De Bruin and Holtslag (1982). We use observations with optimum quality for the period 1 March 1978–1 March 1979, with the sun below the horizon.

From the available data at the micrometeorological field (covered with short grass), we use net radiation, surface radiation temperature and the soil heat flux. Net radiation $Q^*$ is measured with a "Funk"-pyrradiometer. The surface radiation temperature $T_s$ is obtained with a "Heimann"-infrared thermometer installed at about 2 m above the grass surface. The soil heat flux is obtained from heat flux plates and temperature differences in the soil top layer using the method by Slob, as described by De Bruin and Holtslag (1982). This method provides $G_H$ at the surface due to conduction in the soil and ignores the contribution by vapor movement within the soil ($G_v$).

Along the main tower, the temperature profile is available above 20 m. We have used the observations at the 40 and 80 m level. Up to 20 m the temperatures were obtained from the auxiliary mast, as reported by Wessels (1984). In our dataset, total cloud cover $N$ has been taken as the average of four nearby synoptic stations. From the available data at Cabauw we have taken 30 min values around the time of observation of $N$. Observational hours with rain or fog were excluded from the present dataset.

In the present dataset the fluxes of sensible heat and momentum are indirectly derived from observations at an auxiliary mast with the profile method. This method is described by Holtslag (1984) except that Eqs. (10) and (12) are used here for the stability functions of heat and momentum (see section 3c). Below, this method is referred to as method 1. As input to method 1 we use a vertical temperature difference between 10 and 0.5 m, the 10 m wind speed, and an effective surface roughness length $z_0$. The latter is determined with a method by Wieringa (1976). For the Cabauw surroundings $z_0 = 0.15$ m typically, which is substantially larger than values found for uniform grass. Nieuwstadt (1978) showed that the profile method using an effective roughness length, provided fluxes which are in good agreement with fluxes obtained from direct turbulence measurements.

The profile method 1 does not provide the latent heat flux $\lambda E$. For the latter quantity we use data from the homogeneous energy balance field. This is done with a profile method (method 2), using dry and wet bulb temperature differences between 0.45 and 1.1 m, a wind speed at 2 m and the small scale roughness length of grass of $\approx 1$ cm (Wessels 1984). Here it is assumed that the flux profile relations for sensible heat and water vapor transfer are equal. This method is thought to be more reliable than Bowen's ratio method (e.g., Oke 1978), because of the generally low values of $\lambda E$ during nighttime and the large instrumental errors in, e.g., $Q^*$ and $G_H$.

Generally a zero-plane displacement height, $d$, is used in similar methods, as described above. We, however, feel that the use of $d$ is suitable only for homogeneous (tall) vegetation. If levels are used of 10 m or more at Cabauw, the terrain is no longer homogeneous (due to ditches, isolated trees, houses, etc.). On the other hand, the surface energy balance field can be considered almost uniform below $\sim 2$ m. According to Beljaars (1982), Beljaars et al. (1983) and Nieuwstadt (1978), these aspects can be accounted for by using an effective roughness length. Within this empirical approach the concept of $d$ clearly does not fit. Moreover, our model approach (section 3) is meant to describe processes for

the larger scale. Therefore, we decided not to include a zero-plane displacement in our methods. This means that close to the surface the profiles cannot be described very accurately.

In advance we would expect that the larger scale surface inhomogeneities will influence the transfer of momentum (see Brutsaert 1982). Indeed, $u_*$ of method 1 is typically 47% larger than in method 2.

The surface flux of sensible heat is much less influenced by surface inhomogeneities, since these cover a low percentage of the entire surface. Therefore, we expect that the derived values for $H$ with methods 1 and 2 are comparable. A comparison between the two profile methods for the sensible heat flux $H$ provides a rms difference $\sigma = 9.5$ W m$^{-2}$ on an average of $\approx -30.8$ W m$^{-2}$ for method 1 and $-27.7$ W m$^{-2}$ for method 2. (The correlation coefficient $r = 0.78$, and number of observations $n = 131$.) This comparison is illustrated in Fig. 1. The comparison refers to half-hourly values for which the total cloud cover $N \leqq 0.25$.

The relatively large scatter between the two methods for the derivation of $H$ from measurements shows that its value cannot be determined very accurately. For that reason we will compare our model estimates with observations averaged in classes of the "forcing terms", e.g., total cloud cover, temperature at reference height, specific humidity deficit and wind speed.

In order to get an impression of the analyzed dataset, we have listed in Table 1 the observed ranges and averages of the input parameters and some derived quantities. Here $H$ from method 1 is listed and $\lambda E$ from method 2. The data are divided into classes of total cloud cover $N$. In this study we use data at "clear skies" ($N \leqq 0.25$), and "cloudy skies" ($N \geqq 0.75$) only.

TABLE 1. Observed ranges and averages of input parameters and model quantities in the present data set. Upper line refers to clear skies ($N \leqq 0.25$) and lower line to cloudy skies ($N \geqq 0.75$). The averages for $N$ in these classes are 0.13 and 0.88, respectively. The number of observations is $n = 191$ and $n = 312$, respectively. For $\lambda E$ and $T_s$, the numbers are less (see Tables 3a and b).

| Quantity | Symbol | Unit | Range | Average |
|---|---|---|---|---|
| 10-m wind speed | $U_{10}$ | m s$^{-1}$ | 1.0–8.0<br>1.0–9.7 | 3.0<br>4.0 |
| Air temperature at 2 m height | $T_2$ | °C | 1.6–20.6<br>0.8–18.7 | 11.8<br>10.8 |
| Specific humidity deficit at 1.1 m in the air | $\delta q_a$ | g kg$^{-1}$ | 0.3–8<br>0.2–6 | 1.5<br>1.1 |
| Neutral estimate of friction velocity | $u_{*N}$ | m s$^{-1}$ | 0.1–0.8<br>0.1–1.0 | 0.3<br>0.4 |
| Isothermal net radiation | $Q_i^*$ | W m$^{-2}$ | −92–−52<br>−49–−18 | −83<br>−38 |
| Net radiation | $Q^*$ | W m$^{-2}$ | −85–−14<br>−70–5 | −56<br>−22 |
| Surface sensible heat flux | $H$ | W m$^{-2}$ | −72–0<br>−88–0 | −24<br>−22 |
| Surface latent heat flux | $\lambda E$ | W m$^{-2}$ | −22–28<br>−24–52 | −6<br>8 |
| Soil heat flux at the surface due to conduction only | $G_H$ | W m$^{-2}$ | −56–12<br>−38–14 | −20<br>−8 |
| Surface radiation temperature | $T_s$ | °C | −1.0–15.7<br>−4.0–15.1 | 7.9<br>8.4 |
| Air temperature at 50 m height | $T_{50}$ | °C | 3.5–22.1<br>1.3–18.7 | 13.5<br>11.0 |

## 3. The model

### a. General

The surface energy balance over land can be written as

$$H + \lambda E + G = Q^*, \tag{1}$$

where $H$ and $\lambda E$ are the fluxes of sensible and latent heat, respectively (defined positive upwards), $G$ is the soil heat flux and $Q^*$ the net radiation. The latter two energy densities are defined positive downwards.

The net radiation $Q^*$ is the net radiative energy loss that cools the surface relatively to the air and soil layers beneath. So $Q^*$ can be considered as the driving force of the energy balance at the surface (1). During nighttime, $Q^*$ is given by

$$Q^* = L^+ - L^-. \tag{2}$$

Here $L^+$ denotes the incoming longwave radiation from the atmosphere, which is generally governed by the profiles of temperature and humidity in the atmosphere, and the contribution by clouds. This means that $L^+$ can be considered as an independent quantity, which is not directly effected by processes near the surface.

The outgoing longwave radiation from the surface, $L^-$, depends primarily on the surface temperature. It can be regarded as a dependent quantity, since the surface temperature is also related to the surface fluxes of heat and to the soil heat flux. A suitable measure for the independent parameters determining the net radiation is the isothermal net radiation, $Q_i^*$. This is the net (longwave) radiation that would occur at the surface, if the air in the lower atmosphere, between a reference level $z_r$ and the surface is isothermal (Monteith 1981).

Due to radiative cooling at the surface, generally the air will be stably stratified. This implies that turbulence generated by surface friction, will be weakened. For small wind speeds this results in weak turbulence and, therefore, low values for the fluxes of sensible and latent heat are expected. At the same time, large gradients occur in the profiles of wind, temperature and humidity. For larger wind speeds, the gradients are less and

the fluxes are larger. These phenomena will be described with flux-profile relationships.

Due to the radiative cooling at night, the surface temperature may fall below that of the contacting moist air. The ensuing condensation on the surface gives rise to an inverted vapor lapse rate so that turbulence leads to a downward flux of water vapor, known as dew fall (Oke 1978). This phenomenon is confined to a limited range of wind speeds. For small wind speeds, turbulence cannot be maintained and dew fall vanishes. On the other hand, for larger wind speeds the surface does not cool very much compared to the levels above. This means that no new dew fall occurs, and that, in fact, the water vapor transfer can be upwards. In this respect, the nocturnal situation differs from the daytime one, since, generally, only evaporation occurs then.

An important feature of the nocturnal energy balance is that the soil heat flux $G$ is not small compared to the other energy budget terms; moreover, $G$ is not fully understood. In particular, the contribution of water and water vapor transport in the soil to $G$ is not completely known and rather difficult to model (Ten Berge 1986). Another complication is that $G$ depends on soil parameters (such as thermal conductivity and heat capacity), which show a large spatial variability. For these reasons we will describe the soil heat flux semiempirically.

The condensation of water vapor from the soil at the vegetation of the surface is called *destillation* or *dew rise* (Monteith 1963). At low wind speeds dew rise can be as effective as dew fall to wet the vegetation. We will account for dew rise in our approach in a simple empirical way. Unfortunately, no direct measurements of dew rise are available in our dataset.

The quantities of the surface radiation and energy budget are related to the temperature profiles of the atmospheric surface layer and within the soil. In our model, these profiles are described as shown in Fig. 2. First, we distinguish the surface radiation temperature $T_s$, which is thought at a level within the vegetation layer. Secondly, we define $T_0$ as the temperature at the level of the surface roughness length for momentum $z_0$. Next, $T_a$ is the air temperature at screen height ($z_a$) and $T_r$ the air temperature at a reference height $z_r$. The latter height is chosen above the layer in which normally strong temperature gradients occur. Here we took $z_r = 50$ m.

We propose parameterizations and relations for all the quantities of the surface radiation and energy budget, in terms of the temperatures shown in Fig. 2 and other input data. With these assumptions we can solve the surface energy balance in relation to the atmospheric temperature profile up to $z_r$ (see section 5).

### b. The net radiation

The incoming longwave radiation, $L^+$, can be written as

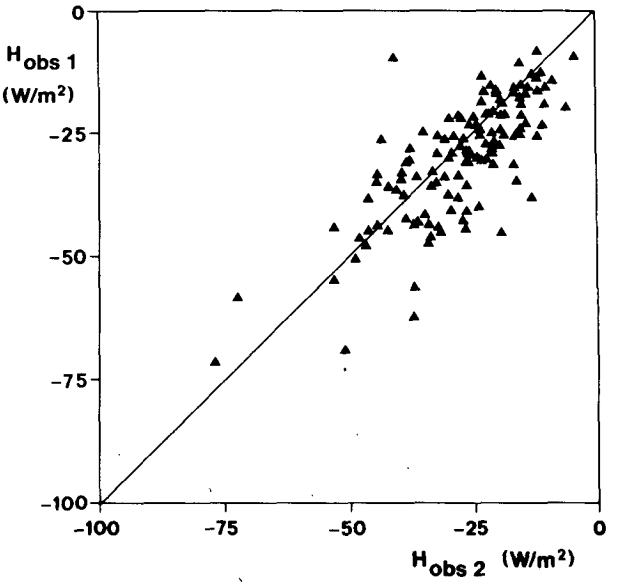


FIG. 1. A comparison between the sensible heat fluxes derived with profile method 1 ($H_{obs1}$) and profile method 2 ($H_{obs2}$) using the available observations ($\sigma = 9.5$ W m$^{-2}$).

$$L^+ = \epsilon_r \sigma T_r^4, \tag{3}$$

where $\epsilon_r$ is the apparent emissivity of the atmosphere, $\sigma$ the Stefan-Bolzmann's constant and $T_r$ the air temperature at level $z_r$.

With clear skies, $L^+$ is determined by the contribution of the gaseous atmosphere (mainly water vapor and carbon dioxide). A suitable parameterization of the emissivity for clear skies, $\epsilon_{r0}$, is given by Swinbank (1963):

$$\epsilon_{r0} = c_1 T_r^2, \tag{3a}$$

where $c_1 = 9.35 \times 10^{-6}$ K$^{-2}$ is an empirical constant. Often the screen height (1–2 m) temperature is used instead of $T_r$. As discussed by Swinbank (1964), however, $T_r$ should be taken above the layer where strong temperature gradients occur. Van Ulden and Holtslag (1983, 1985) found that $z_r = 50$ m is a suitable choice.

In the presence of clouds, $L^+$ increases. For midlatitudes, Paltridge and Platt (1976) proposed

$$\epsilon_r = \epsilon_{r0} + c_2 N/\sigma T_r^4, \tag{3b}$$

where $N$ is total cloud cover, $\epsilon_{r0}$ is given by (3a), and $c_2 = 60$ W m$^{-2}$. For $T_r = 280$ K, we obtain [with Eqs. (3a) and 3b)] $\epsilon_r = 0.73$ at clear skies ($N = 0$) ranging up to $\epsilon_r = 0.90$ at total overcast ($N = 1$).

We compared estimates of $L^+$ given by Eqs. (3)–(3b) with $L^+$ obtained from observations. For the estimates we have used the temperature at 50 m height (interpolated between 40 and 80 m temperature observations). Since, direct measurements of $L^+$ appear to be unreliable (Wessels 1984), we took $Q^* + \sigma T_s^4$ as the "observed" value where $Q^*$ and $T_s$ are observed at the

micrometeorological field. We note that this will introduce additional inaccuracy in our comparison for $L^+$. Both for clear and cloudy skies ($N \leqslant 0.25$ and $N \geqslant 0.75$, respectively) no systematic errors were found, whereas the rms error was 15 and 18 W m$^{-2}$, respectively. (The mean values appear to be 300 and 340 W m$^{-2}$, respectively.)

If the temperature at screen height is used in Eqs. (3)–(3b), the rms error is only slightly larger at clear skies ($\sigma = 16$ W m$^{-2}$). However, $L^+$ is underestimated by $\sim 10$ W m$^{-2}$. These results give some support to Swinbank's (1964) arguments for using a temperature above screen height. For further comparisons we refer to section 5.

In literature, the $\epsilon_r$ in Eq. (3) is often corrected for the influence of water vapor on the incoming longwave radiation. In our dataset, however, no significant variation of $L^+$ with water vapor pressure could be detected. An explanation is that in our dataset the relative humidity (RH) always exceeds 60% (at 1.1 m). By plotting $\epsilon_r$ according to, e.g., Brunt (1932) and Brutsaert (1975), against RH for different temperatures, it can be seen that $\epsilon_r$ is primarily determined by temperature for RH $\geqslant$ 60%. For lower values of the relative humidity a moisture influence in $\epsilon_r$ might be relevant, see, e.g., Brutsaert (1982).

The outgoing longwave radiation from the surface $L^-$ is given by Stefan-Boltzmann's law as

$$L^- = \epsilon_s \sigma T_s^4, \tag{4}$$

where $\epsilon_s$ is the emissivity of the surface and $\sigma$ the Stefan-Boltzmann's constant. For grass, a good approximation is $\epsilon_s = 1$ (Brutsaert 1982), and this value is adopted here.

Combination of Eqs. (2)–(4) provides an expression for the net radiation $Q^*$, which can be linearized. This results in

$$Q^* = Q_i^* + 4\sigma T_r^3 (T_r - T_s)\epsilon_s, \tag{5}$$

where $Q_i^*$ is defined by

$$Q_i^* = -\sigma T_r^4 (\epsilon_s - \epsilon_r). \tag{5a}$$

Here $Q_i^*$ is the isothermal net longwave radiation (Monteith 1981). The last term in Eq. (5) accounts for the temperature difference that normally occurs between $z_r$ and the surface. As discussed by Van Ulden and Holtslag (1983, 1985), this term is important under stable conditions.

### c. *The temperature profile in the lower atmosphere*

In the atmospheric surface layer a temperature difference $T_2 - T_1$ between two levels $z_2$ and $z_1$ is given by (Monin and Yaglom 1971):

$$T_2 - T_1 = \frac{\theta_*}{k}\left[\ln\left(\frac{z_2}{z_1}\right) - \psi_H\left(\frac{z_2}{L}\right) + \psi_H\left(\frac{z_1}{L}\right)\right] - \Gamma_d(z_2 - z_1), \tag{6}$$

where $k$ is the Von Kármán constant, $\Gamma_d$ the dry adiabatic lapse rate and $\psi_H$ a function of $z$ and the Obukhov length scale $L$, defined by (Obukhov 1946)

$$L = \frac{u_*^2}{k\frac{g}{T}\theta_*}. \tag{7}$$

Here $g$ is the acceleration of gravity and $T$ absolute air temperature (at $z = z_a$, for instance). Furthermore, $\theta_*$ is the turbulent temperature scale, which follows from

$$H = -\rho C_p u_* \theta_*, \tag{8}$$

where $\rho C_p$ is the volumetric heat capacity of the air at constant pressure and $u_*$ is the friction velocity.

The friction velocity $u_*$ can be related to a wind speed $U_z$ at level $z$ by a similar expression as (6):

$$u_* = \frac{kU_z}{\ln\left(\frac{z}{z_0}\right) - \psi_M\left(\frac{z}{L}\right) + \psi_M\left(\frac{z_0}{L}\right)}, \tag{9}$$

where $z_0$ and $\psi_M$ are the surface roughness length and the stability function for momentum, respectively.

For the atmospheric surface layer, the stability functions $\psi_H$ and $\psi_M$ are usually given by

$$\psi_H = \psi_M \tag{10}$$

and

$$\psi_M = -5\, z/L, \tag{11}$$

which are adequate for $z/L \leqslant 0.5$ (e.g., Dyer 1974). For larger values of $z/L$, several empirical forms are proposed in literature. Carson and Richards (1978) reviewed the topic and concluded that (10) remains applicable and that the findings of Hicks (1976) are most suitable to describe $\psi_M$. The latter has been confirmed by Holtslag (1984) for Cabauw wind profiles up to $z/L \approx 10$.

Carson and Richards (1978) also proposed analytical approximations to the findings of Hicks (1976) in three intervals of $z/L$. We have found that one expression is able to describe their results:

$$-\psi_M = a\frac{z}{L} + b\left(\frac{z}{L} - \frac{c}{d}\right)\exp\left(-d\frac{z}{L}\right) + \frac{bc}{d}, \tag{12}$$

where $a = 0.7$, $b = 0.75$, $c = 5$ and $d = 0.35$. Equation (12) is similar to the one proposed by Van Ulden and Holtslag (1985) for $z/L \leqslant 10$. For larger values of $z/L$, Eq. (12) results in linear profiles for wind and temperature if it is used in combination with Eqs. (9) and (6), respectively (see section 4).

With (6), (10) and (12), it is possible to describe the temperature profile above the surface layer semiempirically. An experimental verification with our data is given in section 6.

### d. *The surface fluxes of sensible and latent heat*

The surface fluxes of sensible and latent heat can be evaluated with resistance or transfer equations between

the surface and a level in the atmospheric surface layer. Combination of the latter formulations with the energy balance of Eq. (1) leads to a "combination" equation for $\lambda E$, which can be written as (Slatyer and McIlroy 1961; Monteith 1981)

$$\lambda E = \frac{s}{s+\gamma}(Q^* - G) + \frac{\rho c_p}{s+\gamma}(\delta q_a - \delta q_s)D_{sa}u_*. \tag{13}$$

Here $s$ is the slope of the saturation specific humidity curve ($s = \partial q_{sat}/\partial T$), $\gamma$ the psychrometer constant ($\gamma = C_p/\lambda$), and $\delta q_a$ and $\delta q_s$ are defined by

$$\delta q_i = q_{sat}(T_i) - q_i, \tag{14a}$$

where $q_{sat}(T_i)$ is the saturation specific humidity at temperature $T_i$ ($i = s, a$). The specific humidity deficit of the air $\delta q_a$ can be written as

$$\delta q_a = (s+\gamma)(T_a - T_{wa}), \tag{14b}$$

where $T_{wa}$ is the wet bulb temperature of the air at $z_a$.

Furthermore, $D_{sa}$ of Eq. (13) is a transfer coefficient for the air between the surface and level $z_a$ within the surface layer. Often, $D_{sa}u_*$ is written as $1/r_a$, where $r_a$ is the aerodynamic resistance for sensible and latent heat. We prefer the use of $D_{sa}u_*$ because then the influence of $u_*$ on $\lambda E$ is made explicitly.

The sensible heat flux density reads as

$$H = -\rho c_p D_{sa}u_*(\theta_a - T_s), \tag{15}$$

where $\theta_a = T_a + \Gamma_d z_a$. It is assumed that $D_{sa}$ is equal for latent and sensible heat transfer. We will evaluate $D_{sa}$ with our data in the subsection 3e.

Note that Eq. (13) is similar to the usual Penman-Monteith equation (Monteith 1981). The advantage of Eq. (13) is that some special cases are more easily recognized. For instance, in equilibrium conditions with a constant specific saturation deficit, e.g., $\delta q_a = \delta q_s$, we note that the second term of the right-hand side (RHS) of Eq. (13) cancels. In such cases the Bowen ratio is given by $B_0 = H/\lambda E = \gamma/s$. The latter expression is only a function of temperature and this equation can be used as a first estimate of $B_0$ in practical situations (Priestley and Taylor 1972; De Bruin and Holtslag 1982).

In connection with nighttime dew fall above a land surface, Monteith (1963) has called the equilibrium value $\lambda E = \frac{s}{s+\gamma}(Q^* - G)$, the "potential" rate of dew formation. From Eq (3) it follows that this is the maximum fall from the atmosphere on the vegetation. For clear sky conditions and $G = 0$, the maximum value is about 0.07 mm $h^{-1}$ of water, which is equivalent to $-\lambda E \approx 50$ W $m^{-2}$. For the Wangara experiments, Hicks (1983) confirms that this maximum fall is never exceeded. This can be explained by the fact that normally $G \neq 0$ and $\delta q_a > \delta q_s$. Here we note that for dew fall the surface will be close to saturation, e.g., $\delta q_s = 0$.

For large values of $\delta q_a - \delta q_s$ or $u_*$, $\lambda E$ can be positive due to transpiration of the vegetation. In that case,

$$\delta q_s = \frac{\gamma \lambda E}{\rho C_p} r_c, \tag{16}$$

where $r_c$ is the canopy resistance (Monteith 1981). During nighttime $r_c$ is expected to be large. After experimentation with different values we have adopted $r_c = 500$ s $m^{-1}$. The total evaporation from the surface is calculated as the sum of the transpiration from the vegetation and the contribution of the vapor flux from the soil (see below). Results are presented in section 5.

### e. The transfer coefficient $D_{sa}$

In subsection 3d we have defined a transfer coefficient $D_{sa}$ between the surface and a level $z_a$ in the surface layer. From (8) and (15) it follows that $(\theta_a - T_s)/\theta_* = D_{sa}^{-1}$. Since $\theta_a - T_s = (\theta_a - T_0) + (T_0 - T_s)$ we may write

$$\frac{1}{D_{sa}} = \frac{\theta_a - T_0}{\theta_*} + \frac{T_0 - T_s}{\theta_*}, \tag{17}$$

where the temperatures are given in Fig. 2. Equation (17) shows that $(D_{sa})^{-1}$ refers to the transfer processes of two adjacent layers. The first term at the RHS of Eq. (17) is the normalized temperature difference across the lower part of the surface layer and is described by Eq. (6) between $z_2 = z_a$ and $z_1 = z_0$.

For the evaluation of the second term at the RHS of (17), we followed an empirical approach; $T_0$ is derived by extrapolating Eq. (6) downwards to the level of the effective surface roughness length of momentum $z_0$. This is done by using observations of air temperature at 2 m and the fluxes derived with profile method 1 (section 2). The $T_s$ is measured directly with a infrared thermometer installed a few meters above the surface (Wessels 1984). Analyzing the available dataset we found that

$$\frac{T_0 - T_s}{\theta_*} = c_v + \frac{u_0}{u_*}, \tag{18}$$

where $c_v$ and $u_0$ are empirical coefficients. In Fig. 3, Eq. (18) is indicated with $c_v = 10$ and $u_0 = 4.2$ m $s^{-1}$. Probably $c_v$ and $u_0$ are dependent on the surface roughness length $z_0$ and on transfer mechanisms within the canopy sublayer. Unfortunately, our data do not allow further examination.

From Fig. 3 it can be seen that Eq. (18) describes the observations reasonably well up to $u_* \approx 0.4$ m $s^{-1}$. In this figure the observations are represented by averages in classes of $u_*$. The indicated error bars are obtained with $\sigma/\sqrt{n}$, where $\sigma$ is standard deviation and $n$ the number of observations within each class.

The sudden increase of $(T_0 - T_s)/\theta_*$ for low $u_*$ is striking. On the average, $(T_0 - T_s) \approx 6$ K for $u_* \approx 0.05$ m $s^{-1}$ indicating strong temperature differences appear

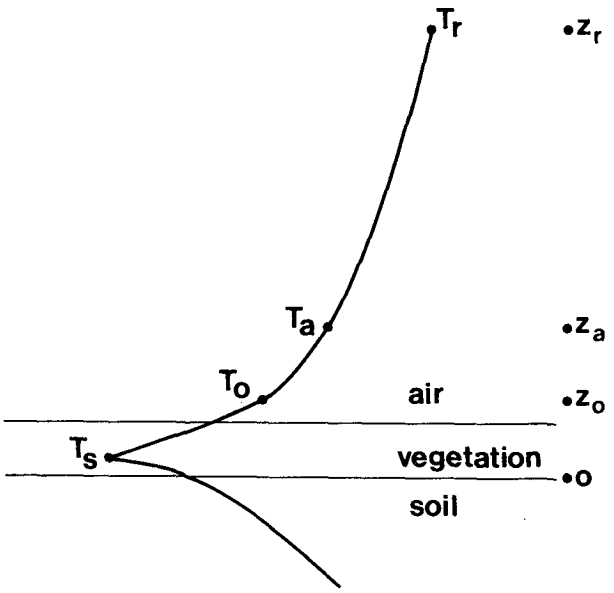


FIG. 2. Schematic view of the temperature profile with indicated temperatures as explained in the text. The heights above the soil surface are indicated at the right hand side.

within the canopy sublayer at low wind speed. For $u_* > 0.3$ m s$^{-1}$ our results show $(T_0 - T_s) \approx 1 - 2$ K.

Often in literature, $(T_0 - T'_s)/\theta_* = B^{-1}$ is denoted (e.g., Garratt and Hicks 1973). Here $T'_s$ is the surface temperature which acts as the source or sink for sensible heat. Brutsaert (1982) concludes that typically $B^{-1} \approx 6$ for homogeneous grass-covered surfaces. Our findings, however, show that $(T_0 - T_s)/\theta_* \approx 20$ if $u_* \gtrsim 0.3$ m s$^{-1}$, which is more than three times larger. A similar value has been used by Van Ulden and Holtslag (1983, 1985) for all values of $u_*$.

The difference between our findings and those in literature can probably be explained by the fact that we have used a larger scale roughness length for the derivation of $u_*$, and that $T_s \neq T'_s$. The latter has been obtained also by Keijman and De Bruin (1979) for Cabauw observations during daytime. On the other hand, Garratt (1978) obtained $(T_0 - T_s)/\theta_* \approx 6.2$ during daytime for a heterogeneous surface with a large aerodynamic roughness. This subject certainly needs more investigation. For the time being we adopt Eq. (18) as a practical relation for the estimation of $T_0 - T_s$.

### *f. The total soil heat flux*

During nighttime the soil heat flux $G_z$ is generally directed upwards and is primarily determined by conduction. It is described by

$$G_z = -k_s \frac{\partial T_z}{\partial z}, \tag{19}$$

where $T_z$ is a soil temperature at depth $z$ and $k_s$ is the "apparent" thermal conductivity of the soil. This conductivity may differ from the usual conductivity due to vapor movement in the soil.

Combination of (19) with an equation for conservation of heat in the soil provides the well-known diffusion equation. This equation can be solved for a given initial temperature profile and a boundary condition, which results in a variation of $G_z$ and $T_z$ with $z$ for given properties of the soil (e.g., Groen 1947; Van Wijk and Derksen 1963, Ten Berge 1986). Such a solution of the diffusion equation, however, is rather complicated for practical applications, and most times the required input parameters are not available. For that reason we search for a simple empirical relation for $G$.

In Fig. 4 a comparison is given between observations of $G_H$ (see section 2) and $H$ for the two classes of total cloud cover and two classes of specific humidity deficit in the air at 1.1 m height ($\delta q_a$). All the points represent averages for given values of $H$. It is seen that a linear relation is a fairly good approximation for the two classes of $N$, while the influence of $\delta q_a$ appears to be insignificant. In this way we arrived at

$$G_H = -a_G H + b_G Q_i^*. \tag{20}$$

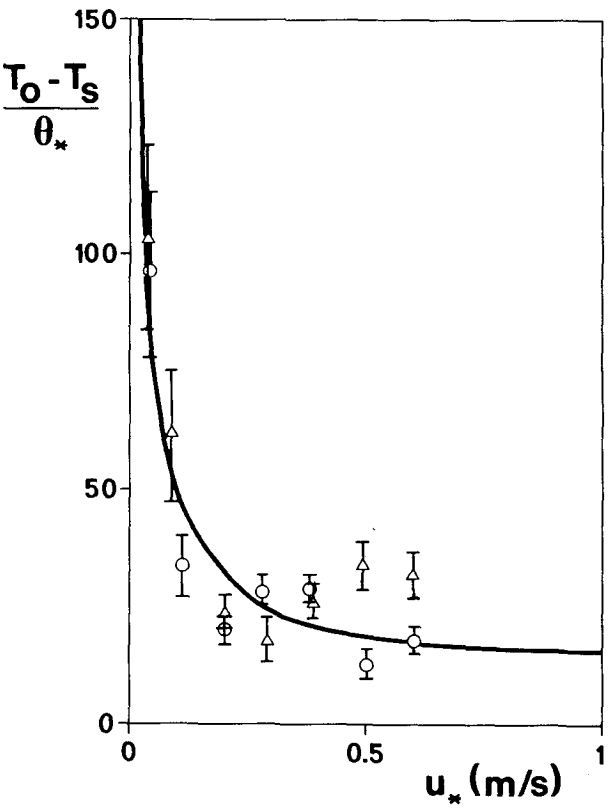


FIG. 3. The normalized temperature difference $(T_0 - T_s)/\theta_*$ near the surface as a function of friction velocity $u_*$ for clear skies ($N \leq 0.25$). A distinction is given for cases with specific humidity deficit $\delta q_a \leq 1$ g kg$^{-1}$ (dots) and $\delta q_a \geq 1$ g kg$^{-1}$ (triangles). The average values for $\delta q_a$ are 0.66 and 2.2 g kg$^{-1}$, respectively. The indicated line is given by Eq. (18).

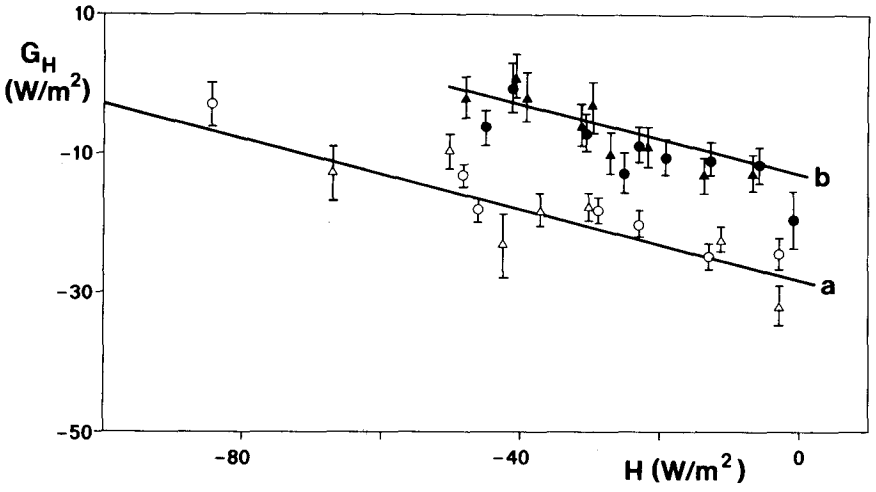


FIG. 4. The soil heat flux due to conduction $G_H$ as a function of sensible heat flux $H$ for (a) clear skies and (b) cloudy skies. A distinction is made in two classes of specific humidity deficit $\delta q_a$ as in Fig. 3. The indicated lines are given by Eq. (20), with $Q_i^* = -83$ W m$^{-2}$ for clear skies and $Q_i^* = -38$ W m$^{-2}$ for cloudy skies.

Here $a_G \approx \frac{1}{4}$, $b_G \approx \frac{1}{3}$, and $Q_i^*$ is the isothermal net radiation of Eq. (5a). The rms error of this estimate is about 8 W m$^{-2}$.

According to Eq. (20), $|G_H|$ and $|H|$ are correlated negatively for given values of $Q_i^*$. This can be explained as follows. If for some reason $T_s$ decreases as a response on an atmospheric forcing, $|G_H|$ will increase due to a larger temperature difference. This is the case, because in the soil the temperature responds more slowly to atmospheric variations than $T_s$. On the other hand, a decrease of $T_s$ relative to $T_r$ means a more stable stratification in the atmospheric surface layer, e.g., $|H|$ decreases. Similarly, an increase of $T_s$ will lead to a decrease of $|G_H|$ and an increase of $|H|$. In very stable conditions Eq. (20) provides $G_H = \frac{1}{3}Q_i^*$. This limit will be discussed in more detail in section 4.

As noted before, $G_H$ of Eq. (20) is the soil heat flux due to conduction only. To account for the influence of the water vapor movement in the soil we write

$$G = G_H + G_v, \tag{21}$$

where $G_v$ is the contribution to vertical heat transfer due to a water vapor flux. For soils with saturated air, Ten Berge (1986) shows that $G_v$ can amount 10% to 25% of $G_H$, while for very dry soils this percentage even can be 50%. A simple parameterization for $G_v$ is, therefore,

$$G_v = c_G G_H. \tag{22}$$

Here we adopt $c_G = 0.2$. We realize that this parameterization is a very simple description of the complicated transfer processes in the soil; $c_G$ can easily vary by a factor of 2.

The final expression for the total heat flux $G$ is

$$G = -a'_G H + b'_G Q_i^*, \tag{23}$$

where $a'_G = a_G(1 + c_G) \approx 0.3$ and $b'_G = b_G(1 + c_G) \approx 0.4$. We expect that this equation is applicable for soils with saturated air, which are covered with short vegetation. Independent verification, however, is recommended.

## 4. The critical wind speed

It is to be expected that when the wind speed drops below a certain value, $U_{cr}$, turbulence cannot be maintained any longer in the surface layer, which means that $u_*$, $\theta_*$ and $L$ will vanish. Due to the difference in emissivities of the atmosphere and the surface, a temperature difference will remain between $z_r$ and the surface. This "critical" temperature difference can be evaluated from the present model equations as follows.

For $U \leqq U_{cr}$ it follows that $H = \lambda E = 0$. According to Eqs. (1), (20), (21), and (23), then $G = Q^*$ and $G = b'_G Q_i^*$. Combining this with Eqs. (5)–(5a) we arrive at

$$\Delta T_{cr} = (T_r - T_s)_{cr} = \frac{(1 - b'_G)}{4}(\epsilon_s - \epsilon_r)T_r. \tag{24}$$

This equation shows that the temperature difference is zero for the hypothetical case $\epsilon_r = \epsilon_s$. Moreover, if $b'_G = 0$ (e.g., $G = Q^* = 0$), the temperature difference is only regulated by emissivity differences between the surface and the atmosphere. This might occur for a surface which is completely isolated from the soil layer beneath. We have found, however, that $b'_G = 0.4$, typically. Combining this with $\epsilon_r = 0.73$ for clear skies (section 3b) we find $\Delta T_{cr} = 11.3$ K for $T_r = 280$ K. For cloudy skies with $\epsilon_r = 0.90$ we arrive at $\Delta T_{cr} = 4.2$ K. These are realistic values, which can occur across the lower atmosphere and canopy layers in very stable conditions.

Alternatively, $T_r - T_s$ is given by Eq. (6) and Eq. (18). In the limit for strong stability, the temperature profile of Eq. (6) is linear and $\psi_H = \psi_M$ is approaching $\psi_H \rightarrow -az/L$ (see Eq. (12)). Combination of this with (6) and (18) provides an equation for $\theta_*/u_*$, which can be written as

$$\left(\frac{\theta_*}{u_*}\right)_{cr} = \frac{u_0}{2(g/T)z_r a}\left[-1 + \left(1 + \frac{4(g/T)az_r\Delta\theta_{cr}}{u_0{}^2}\right)^{1/2}\right]. \tag{25}$$

Here $\Delta\theta_{cr} = \Delta T_{cr} + \Gamma_d z_r$, where $\Delta T_{cr}$ is given by Eq. (24). Equation (25) shows that the critical value of $\theta_*/u_*$ is given by the surface vegetation coefficients and atmospheric parameters. We note that $(\theta_*/u_*)_{cr}$ varies with a square root dependence on the critical temperature difference.

From Eqs. (12) and (9) we also note that in strong stability, the wind profile tends to a linear shape. This implies a critical wind speed $U_{cr}$ at level $z$ given by

$$U_{cr} = az\frac{g}{T}\left(\frac{\theta_*}{u_*}\right)_{cr}. \tag{26}$$

With the above equations we can calculate typical values for $(\theta_*/u_*)_{cr}$ and $U_{cr}$. For instance, if $T_r = 280$ K, $z_r = 50$ m and using the numerical values for the coefficients as proposed in section 3, we arrive at $(\theta_*/u_*)_{cr} = 1.8$ Ks m$^{-1}$ at clear skies ($N = 0$) with $\Delta T_{cr} = 11.3$ K. For the 10 m level then Eq. (26) provides $U_{cr} \approx 0.45$ m s$^{-1}$. For total overcast ($N = 1$) we obtain $(\theta_*/u_*)_{cr} = 0.9$ Ks m$^{-1}$ and $U_{cr} \approx 0.23$ m s$^{-1}$. These values for the critical wind speed are surprisingly low and are close to the threshold wind speed of cup anemometers.

The present results differ from that obtained earlier by Venkatram (1980), using a constant temperature scale $\theta_*$ and $\psi_H = \psi_M = -5z/L$. The latter author arrives at a critical wind speed at 10 m of $U_{cr} \approx 2.5$ m s$^{-1}$. This value is much larger, because in Venkatram's parameterizations $\theta_*$ does not tend to zero for strong stability. Moreover, the $\psi_H$ and $\psi_M$ functions which he used are valid only for $z/L < (0.5 - 1)$ (see section 3c).

Carson and Richards (1978) discuss the influence of different $\psi_M$ and $\psi_H$ functions on a critical bulk Richardson number $\mathrm{Ri}_{B_{cr}}$. For the profile functions of Hicks (1976), as used by us, one obtains

$$\mathrm{Ri}_{B_{cr}} \approx 1/a, \tag{27}$$

where $a$ is the coefficient of Eq. (12). For $a = 0.7$ it follows that $\mathrm{Ri}_{B_{cr}} \approx 1.4$.

## 5. Results

For the calculation of the surface fluxes and the other terms of the proposed model equations we need to specify a single wind speed $U_z$ (usually at 10 m height), the surface roughness length of momentum $z_0$, total cloud cover $N$, and dry and wet bulb temperatures $T_a$ and $T_{wa}$, respectively. The latter two temperatures provide the specific humidity deficit in the air, $\delta q_a$. [See Eqs. (14a) and (14b).]

The model equations can be solved for all terms in the energy budget of Eq. (1), by using Newton-Raphson's iteration method. The iteration is done with help of the Obukhov length $L$, of which an interval is specified. Within this interval, a value of $L$ is sought which balances the terms of (1). Table 2 gives a summary of how the quantities in the scheme are calculated from the equations and the available inputs. The calculation of $\lambda E$ is done with Eq. (13), where initially $\delta q_s = 0$. However, if it appears that $\lambda E > 0$ we use a specified canopy resistance $r_c$ to evaluate $\lambda E$ from Eqs. (13) and (16). This provides the transpiration of the vegetation. In this case the vapor inversion profile in the surface layer is no longer present, which means that the moisture flux from the soil, notably $|G_v|$, is directly available to contribute to the total evaporation. Therefore, the sum of $\lambda E$ of Eq. (13) and $|G_v|$ of Eq. (22) is taken in these cases.

Using the above scheme we finally arrive at all the components of Eq. (1). Iteration with a new value of $L$ is continued, until all the terms of (1) are in equilibrium. This might sometimes take more than ten iteration steps to obtain an accuracy of 1 W m$^{-2}$ in Eq. (1).

The model output can be expressed in terms of $Q_i^*$ (see Eq. (5a)), $\delta q_a$ and $u_{*N}$. The latter is the normalized wind speed at 10 m, which can be obtained from Eq. (9) for $z/L = 0$. These quantities can be considered the independent input parameters. For the simulations we used $z_0 = 0.15$ m, $z_a = 1.1$ m for the level where $\delta q_a$ is specified, and $T_r = 10°$C for $z_r = 50$ m. Normally, however, $T_r$ needs to be calculated from $T_a$ and the other inputs (see Table 2).

In Fig. 5 the dependence of $\theta_*$ on $u_{*N}$ is given for specified values of $\delta q_a$ and $Q_i^* = -83$ W m$^{-2}$. The latter value for $Q_i^*$ corresponds for our dataset to $N = \frac{1}{8}$ and $T_r \approx 10°$C, and is in our dataset representative

TABLE 2. Summary of the calculation procedure for the quantities of the scheme with equation numbers and inputs. The computation is started with a prescribed value of Obukhov length $L$.

| Symbol | Equation nos. | Inputs |
|---|---|---|
| $u_*$ | (9), (12) | $U_z$, $z_0$, $L$ |
| $\theta_*$ | (7) | $u_*$, $L$, $T_a$ |
| $T_r$ | (6) | $T_a$, $L$, $\theta_*$ |
| $T_0$ | (6) | $T_a$, $L$, $\theta_*$, $z_0$ |
| $T_s$ | (18) | $T_0$, $\theta_*$, $u_*$ |
| $Q_i^*$ | (5a), (3b) | $T_r$, $N$ |
| $Q^*$ | (5) | $T_r$, $T_s$, $Q_i^*$ |
| $H$ | (8) | $u_*$, $\theta_*$ |
| $G$ | (23) | $H$, $Q_i^*$ |
| $D_{sa}$ | (17) | $\theta_*$, $T_a$, $T_s$ |
| $\lambda E$ | (13), (16) | $Q^*$, $G$, $\delta q_a$, $u_*$ |

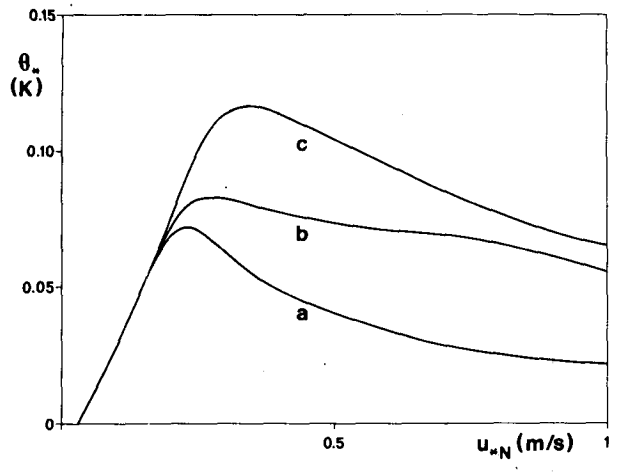


FIG. 5. The dependence of $\theta_*$ on $u_{*N}$ for $Q_i^* = -83$ W m$^{-2}$ as obtained from the model equations (e.g., $N$ = ⅛, $T_r$ = 10°C) for three values of specific humidity deficit, e.g., curve a, $\delta q_a = 0$; curve b, $\delta q_a = 0.66$ g kg$^{-1}$, and curve c, $\delta q_a = 2.2$ g kg$^{-1}$. Here $u_{*N}$ is the normalized 10-m wind speed.

for clear skies. In Fig. 5, three values for $\delta q_a$ are indicated, ranging from a saturated atmosphere (Fig. 5a) to dry conditions (Fig. 5b) with $\delta q_a = 0.66$ g kg$^{-1}$ and $\delta q_a = 2.2$ g kg$^{-1}$ (Fig. 5c). The latter two values are representative for the subdatasets of Figs. 3 and 4.

From Fig. 5 we note the linear dependence of $\theta_*$ on $u_{*N}$ for $u_{*N} \leqslant 0.2$ m s$^{-1}$, irrespective of the value for $\delta q_a$. However, the peak values of the curves are dependent on $\delta q_a$. This is mainly caused by the variation of $\lambda E$ with $\delta q_a$ and $u_{*N}$, as depicted in Fig. 6 for $Q_i^* = -83$ W m$^{-2}$. However, except for saturated conditions ($\delta q_a = 0$), $\lambda E$ is relatively small and $\theta_*$ is not influenced very strongly by $\delta q_a$.

In Fig. 6 the typical behavior of $\lambda E$ is shown for four values of $\delta q_a$. For increasing values of wind speed (e.g., $u_{*N}$), first $\lambda E$ decreases but later it increases to become positive. This behavior can be explained with the aid of Eq. (13), which shows a balance between two relatively large opposite terms (if $\delta q_a > 0$ and $u_* > 0$). The curve of Fig. 6d represents the variation of $\lambda E$ with $u_{*N}$ for $\delta q_a = 1.5$ g kg$^{-1}$. The latter value is typical for our dataset with clear skies (see Table 1). To obtain the curves of Fig. 6 we have used $r_c = 500$ s m$^{-1}$ if $\lambda E > 0$. Tacitly we ignored evaporation from rainwater or dew. Subjectively, the latter value showed the best agreement with our data in clear sky conditions ($N \leqslant 0.25$). If, instead, $r_c = 250$ s m$^{-1}$ is used, we obtain $\lambda E = 12.0$ W m$^{-2}$ and $H = -78.6$ W m$^{-2}$ for $u_{*N} = 1$ m s$^{-1}$ with clear skies. For $r_c = 1000$ s m$^{-1}$ these figures are $\lambda E = 5.0$ W m$^{-2}$ and $H = -70.2$ W m$^{-2}$; therefore a factor 2 change in $r_c$, results in a factor of 1.6 in $\lambda E$. The sensitivity of $H$ (and $Q^*$) is small.

In Fig. 7 we have given the dependence of all the terms in Eq. (1) with $u_{*N}$ for clear sky conditions (i.e., $Q_i^* = -83$ W m$^{-2}$) and $\delta q_a = 1.5$ g kg$^{-1}$. It is seen that the sensible heat flux $H$ shows a large variation with

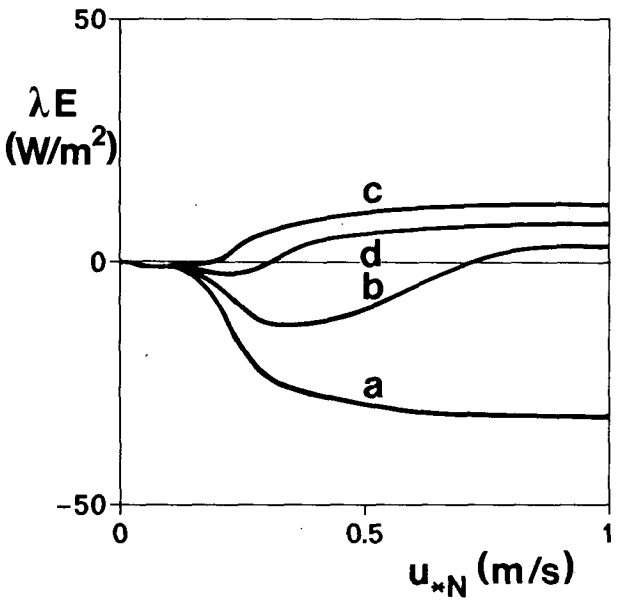


FIG. 6. The dependence of $\lambda E$ on $u_{*N}$ for $Q_i^* = -83$ W m$^{-2}$ as obtained from the model equations. A distinction is made for four values of specific humidity deficit, e.g., curve a, $\delta q_a = 0$; curve b, $\delta q_a = 0.66$ g kg$^{-1}$; curve c, $\delta q_a = 2.2$ g kg$^{-1}$; and curve d, $\delta q_a = 1.5$ g kg$^{-1}$.

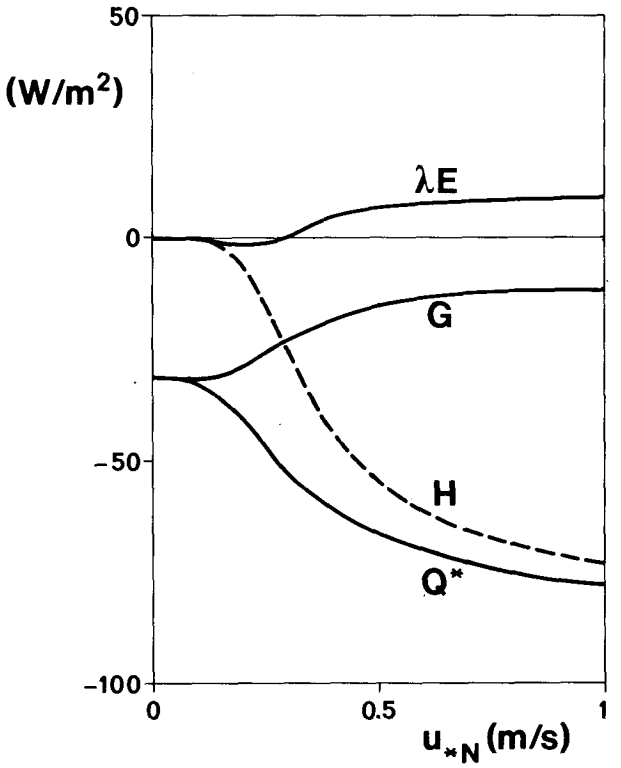


FIG. 7. The variation of $\lambda E$, $G$, $H$ and $Q^*$ with $u_{*N}$ for $Q_i^* = -83$ W m$^{-2}$ (clear skies).

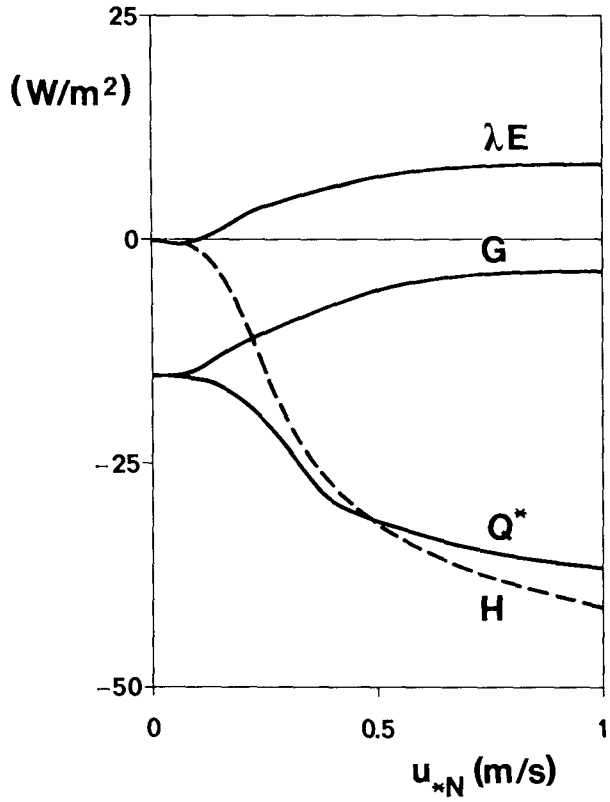


FIG. 8. As in Fig. 7, except for $Q_l^* = -38$ W m$^{-2}$ (cloudy skies).

$u_{*N}$. For large wind speeds the present model equations show that $Q^* \rightarrow Q_l^*$. This means that for large wind speeds $H$ approaches $Q_l^*$ if we neglect $\lambda E$ and $G$ (see Fig. 4). The results for cloudy skies ($N \geqq 0.75$) with $Q_l^* = -38$ W m$^{-2}$ are illustrated in Fig. 8. It shows similar behavior to Fig. 7 for the terms in the surface energy budget.

In Fig. 9 the dependence of $\theta_*$ on $u_{*N}$ for $\delta q_a = 1.5$ g kg$^{-1}$ is shown. Distinction is made for three values of $Q_l^*$. From this figure we note that the maximum values of $\theta_*$ vary strongly with $Q_l^*$ (i.e., $N$). This result is consistent with the findings of Holtslag and Van Ulden (1982).

In Tables 3a and b a comparison is given for $u_*$, $\theta_*$, $H$, $\lambda E$, $Q^*$, $G_H$ and $T_s$, obtained from observations and the model equations. A distinction is made between clear skies ($N \leqq 0.25$) and cloudy skies ($N \geqq 0.75$). In these tables the derived values for $u_*$, $\theta_*$ and $H$ from profile method 1 are used for comparison with the values of the scheme. Since in method 1 the same 10 m wind speed and roughness length are used as in our model calculations, some bias will be apparent. The same is true when we compare $H$ (and $\lambda E$) of the scheme with the derived values of profile method 2. In that case the specific humidity deficit is a common quantity. Such a comparison leads to the same skill for $H$ as for the comparison with profile method 1 (see table 3a). In section 2 it is shown that a comparison of the two profile methods with different input data leads

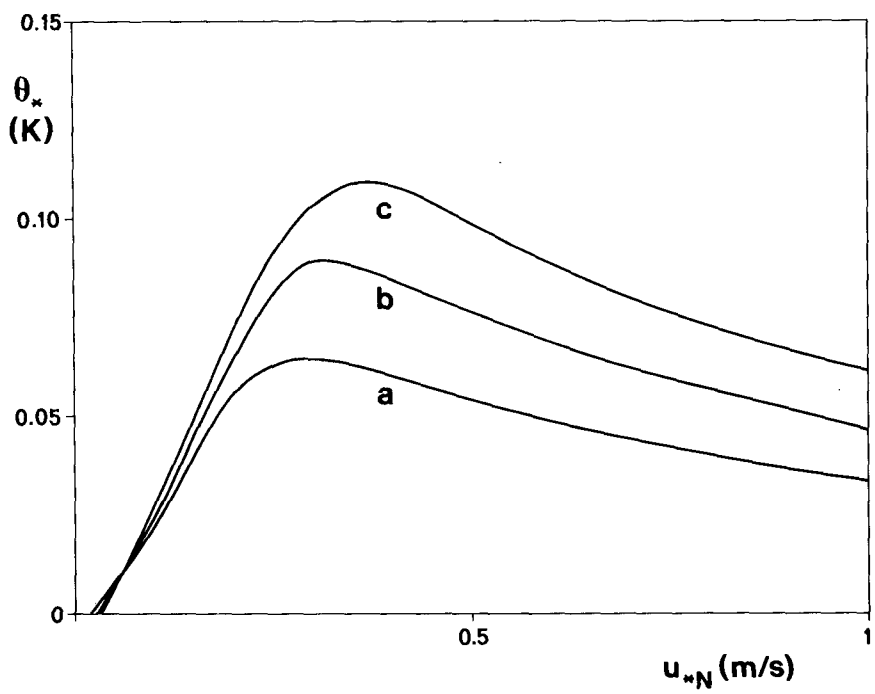


FIG. 9. The dependence of $\theta_*$ on $U_{*N}$ for $\delta q_a = 1.5$ g kg$^{-1}$ as obtained from the model equations. A distinction is made for three values of cloud cover with $T_r = 10$°C, e.g., curve a, $N = \frac{7}{8}$ ($Q_l^* = -38$ W m$^{-2}$); curve b, $N = \frac{4}{8}$ ($Q_l^* = -60$ W m$^{-2}$); and curve c, $N = \frac{1}{8}$ ($Q_l^* = -83$ W m$^{-2}$).

TABLE 3. Comparison of model estimates with observations for clear and cloudy skies. Here $n$ is number of observations, $\bar{x}$ the average of calculations, $\bar{y}$ the average of observations; $\sigma$ rms error and $r$ correlation coefficient. Units are K for $\theta_*$, °C for $T_s$, m s$^{-1}$ for $u_*$, and W m$^{-2}$ for the other terms.

| Parameter | $u_*$ | $\theta_*$ | $H$ | $\lambda E$ | $G_H$ | $Q^*$ | $T_s$ |
|---|---|---|---|---|---|---|---|
| | | | a. *Clear skies* ($N \leq 0.25$) | | | | |
| $n$ | 191 | 191 | 191 | 131 | 191 | 191 | 134 |
| $\bar{x}$ | 0.22 | 0.086 | −24.0 | −4.5 | −21.0 | −54.0 | 7.6 |
| $\bar{y}$ | 0.21 | 0.095 | −24.3 | −5.8 | −19.5 | −55.9 | 7.9 |
| $\sigma$ | 0.03 | 0.028 | 6.3 | 5.6 | 8.9 | 12.9 | 1.8 |
| $r$ | 0.98 | 0.43 | 0.91 | 0.86 | 0.33 | 0.33 | 0.92 |
| | | | b. *Cloudy skies* ($N \geq 0.75$) | | | | |
| $n$ | 312 | 312 | 312 | 291 | 312 | 312 | 210 |
| $\bar{x}$ | 0.37 | 0.045 | −20.0 | 1.8 | −7.4 | −27.4 | 7.8 |
| $\bar{y}$ | 0.36 | 0.050 | −22.3 | 8.3 | −8.4 | −22.0 | 8.4 |
| $\sigma$ | 0.02 | 0.021 | 9.3 | 12.0 | 7.5 | 16.1 | 1.7 |
| $r$ | 0.99 | 0.35 | 0.78 | 0.70 | 0.44 | 0.25 | 0.93 |

to $\sigma \approx 9.5$ W m$^{-2}$, which is slightly larger than the value of Table 3a (see Fig. 1).

In Fig. 10 and 11, a comparison is given between the estimates for the sensible heat flux with the ones derived from the two profile methods. In Figs. 12 and 13, a similar comparison is given for $\lambda E$ and $u_*$. All these comparisons are for clear skies ($N \leqq 0.25$) only. From the latter figures, and Tables 3a and b, it can be seen that, on average, the agreement is good between observations and estimates, but that a large difference may occur between individual observations and model estimates. Possibly, the skill for $\lambda E$ under cloudy conditions can be improved by taking a smaller value for $r_c$ (larger $\lambda E$ if $\lambda E > 0$). This approach is not followed here, because of the large uncertainty in $\lambda E$ under these conditions.

In Fig. 14, a comparison is given between observations and estimates of net radiation at clear skies. From this figure and tables 3a and b it can be seen that the agreement is not very good. Partly, this will be caused by observation errors in net radiation, which during nighttime are certainly of the order of 10 W m$^{-2}$. But the disagreement will also be due to imperfection of our model. Since the surface radiation temperature $T_s$ is described very well by our approach (see tables 3a and b) and Eq. (4) is generally accepted to describe $L^-$, the main errors must be due to the parameterization of $L^+$ (Eqs. (3)–(3b)). On the other hand, the temperature at 50 m is also well described by our approach

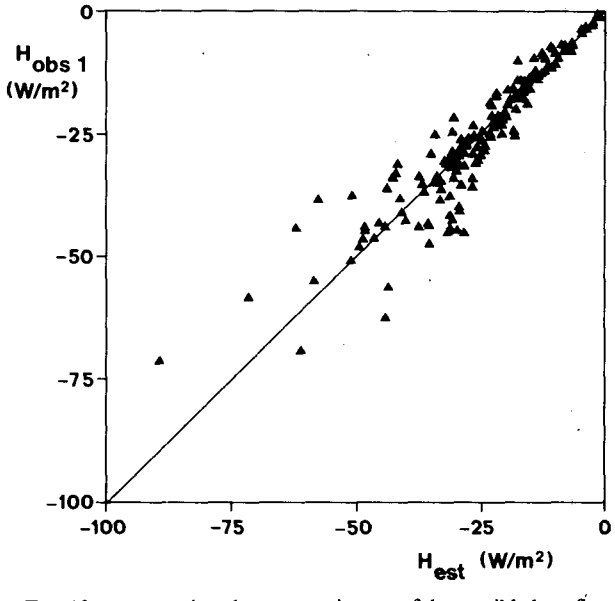


FIG. 10. A comparison between estimates of the sensible heat flux ($H_{est}$) and values derived with profile method 1 ($H_{obs1}$) for clear skies ($N \leqq 0.25$). Here $\sigma = 6.3$ W m$^{-2}$.

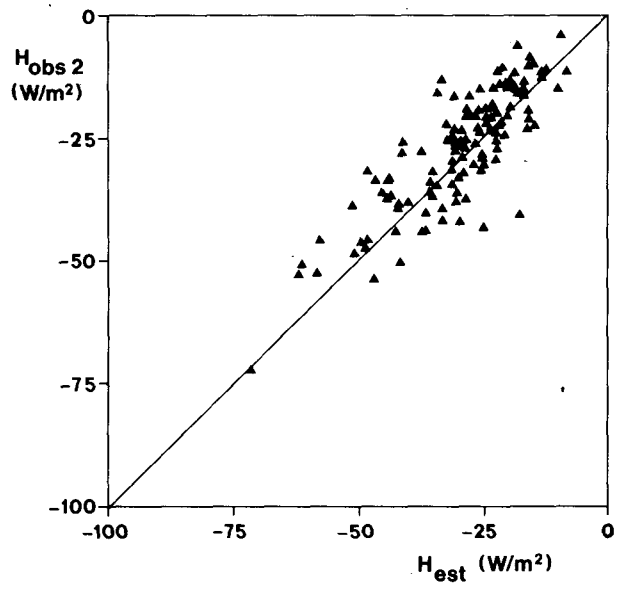


FIG. 11. As in Fig. 10 for profile method 2 ($\sigma = 7.2$ W m$^{-2}$).

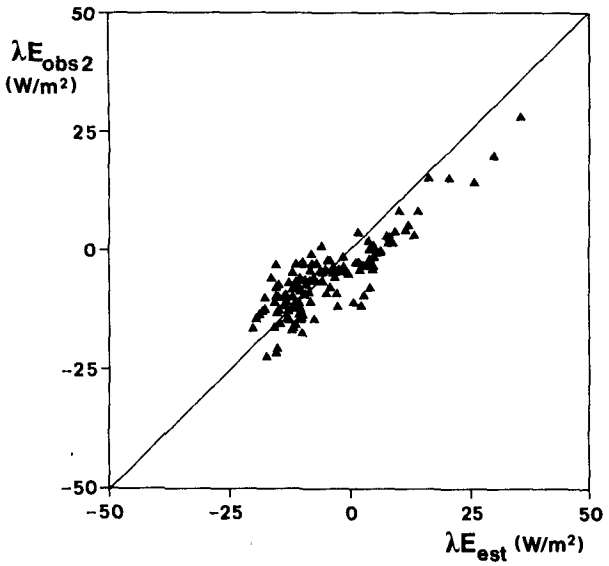


FIG. 12. As in Fig. 11 for the latent heat flux $\lambda E$ ($\sigma$ = 5.6 W m$^{-2}$).

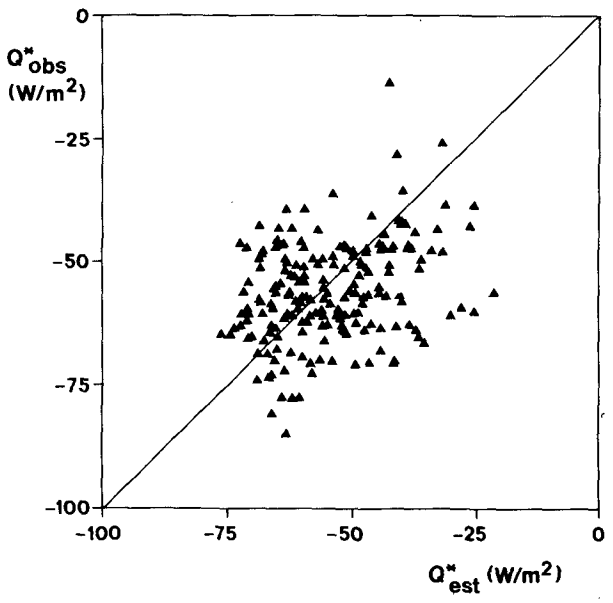


FIG. 14. A comparison between estimates ($Q^*_{est}$) and observations ($Q^*_{obs}$) for the net radiation at clear skies ($\sigma$ = 12.9 W m$^{-2}$).

(see section 6). This implies that parameterizations such as Eq. (3a), using the temperature at one level, possibly are too simple. However, it must be realized that $Q^*$ is a difference of two large quantities ($L^+$ and $L^-$), so errors in estimates of $Q^*$ will always be considerable.

## 6. Simulation of the temperature profile

As a part of the present scheme the temperature profile is described with Eqs. (6), (10) and (12). In tables 4a and b a comparison is given between the temperature observations and calculations at five heights for the two classes of total cloud cover. For the calculations we used the observed temperature at 2 m, the fluxes of the present scheme and the above mentioned equations. So, only routine weather data were used as input variables.

From Tables 4a and b it is seen that the agreement between observations and calculations is surprisingly good. However, the skill decreases with increasing height. An illustration of the generally good agreement is shown in Fig. 15 for clear skies. At each level error bars are indicated for the temperature observations (e.g., $\sigma/\sqrt{n}$). The data are divided into three classes of stability, defined with Obukhov length $L$ as $45 \leqq L < 90$ (Fig. 15a), $20 \leqq L < 45$ (Fig. 15b), and $5 \leqq L < 20$ (Fig. 15c). Mean values for the Obukhov length are 54, 29 and 12 m, respectively.

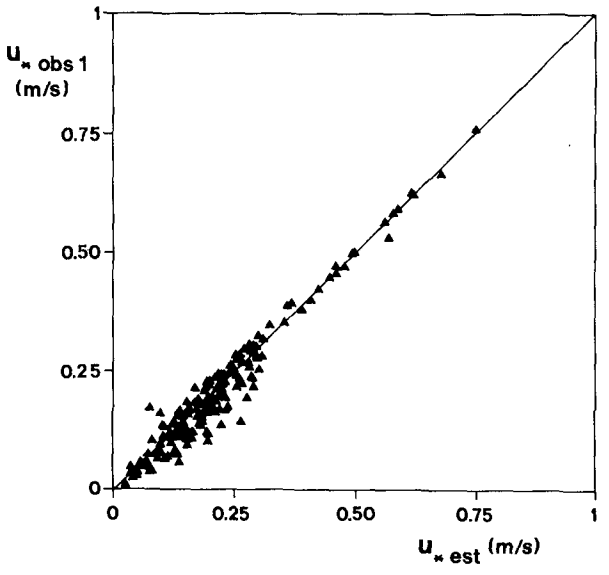


FIG. 13. As in Fig. 10 for the friction velocity $u_*$ ($\sigma$ = 0.03 m s$^{-1}$).

TABLE 4. Comparison of model estimates with Cabauw temperature observations at different heights ($z$) up to 80 m. All data are used. Symbols are as in tables 3a, b; units are in °C.

| | $z$ (m) | | | | |
|---|---|---|---|---|---|
| Parameter | 5 | 10 | 20 | 40 | 80 |
| | a. *Clear skies* ($N \leqslant 0.25$) | | | | |
| $n$ | 191 | 191 | 191 | 191 | 191 |
| $\bar{x}$ | 12.1 | 12.4 | 12.8 | 13.3 | 13.7 |
| $\bar{y}$ | 12.2 | 12.4 | 12.7 | 13.3 | 14.2 |
| $\sigma$ | 0.24 | 0.42 | 0.59 | 0.81 | 1.50 |
| $r$ | 0.99 | 0.99 | 0.99 | 0.98 | 0.94 |
| | b. *Cloudy skies* ($N \geqslant 0.75$) | | | | |
| $n$ | 312 | 312 | 312 | 312 | 312 |
| $\bar{x}$ | 10.9 | 10.9 | 11.0 | 10.9 | 10.8 |
| $\bar{y}$ | 10.9 | 11.0 | 11.0 | 11.0 | 11.0 |
| $\sigma$ | 0.10 | 0.17 | 0.25 | 0.42 | 0.79 |
| $r$ | 0.99 | 0.99 | 0.99 | 0.99 | 0.99 |

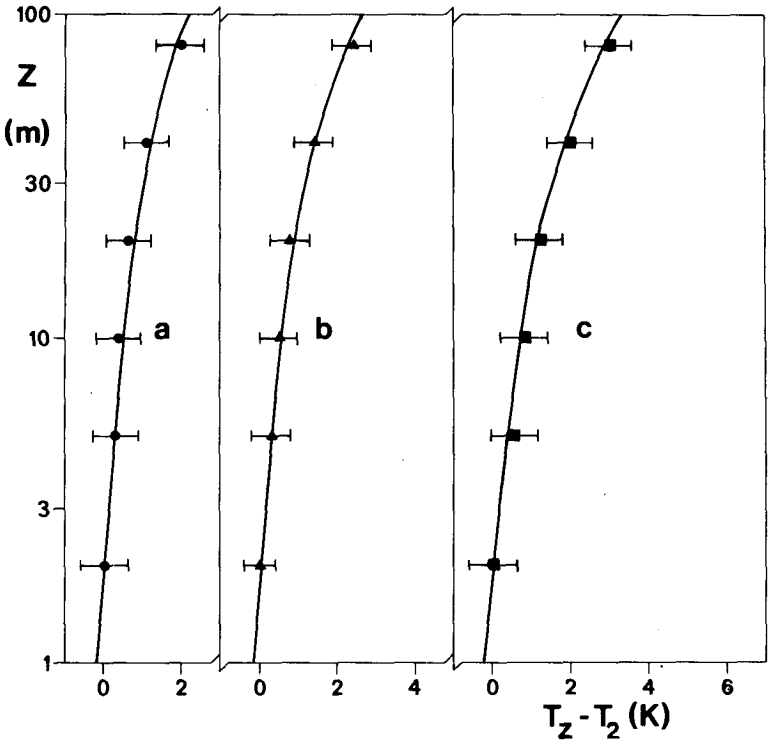


FIG. 15. The temperature profile at Cabauw, averaged in three classes of stability: curve a, $L$ = 57 m, $\theta_*$ = 0.10 K; curve b, $L$ = 26 m, $\theta_*$ = 0.09 K; and curve c, $L$ = 12 m, $\theta_*$ = 0.08 K. The curves are obtained from Eqs. (6), (10) and (12) and with the use of the modeled surface fluxes. The indicated error bars represent twice the standard deviation of the temperatures $T_z$ (not $T_z - T_2$) at each level.

From the evidence shown in Tables 4 and Fig. 15, we conclude that the scheme with the chosen stability functions is suitable to desscribe the nocturnal temperature profile up to 80 m. This corresponds, on average, to $z/L \approx 7$ in Fig. 15c. This seems surprising at first, because we used surface-layer variables for the description of the temperature profile. An explanation for this discrepancy is that above the surface layer the temperature profile is determined by the local Obukhov length and the local fluxes (Nieuwstadt 1984a), which are often closely related to their surface values (Holtslag and Nieuwstadt 1986). Apparently these relationships are incorporated in the stability function of Eq. (12). Similar findings for the wind profile at Cabauw were obtained by Holtslag (1984).

For $z/L > 5$–10, intermittent turbulence will occur in the NABL (Holtslag and Nieuwstadt 1986) and Eq. (12) is expected to be unreliable. In such cases also the exchange coefficients for heat and momentum may be different, e.g., $\psi_H \neq \psi_M$ (Turner 1973; Hicks 1976; Kondo et al. 1978). Also, divergence of radiation appears to be significant above the turbulent layer (Estournel and Guedalia 1985).

These results imply that with our choice for $z_r$ = 50 m, the fluxes of our scheme are less reliable for $L < 5$–10 m. The latter corresponds to very low values for $u_*$ and $\theta_*$ ($u_* < 0.07$ m s$^{-1}$ and $\theta_* < 0.07$ K). On the other hand, however, we have found that when the reference height $z_r$ is chosen below a height of approximately 30 m, serious errors are introduced in the simulation of the temperature profile.

## 7. Summary and discussion

In this paper we have presented a semiempirical scheme, which relates the surface fluxes to routine weather variables during nighttime over land. The routine weather variables are total cloud cover, wind speed and wet and dry bulb temperature of the air. The latter three variables are only needed at a single height in the atmospheric surface layer (below 50 m). Observations above a grass-covered surface in Cabauw, The Netherlands, are used to design some of the parameterizations and to investigate findings from literature. In the scheme parameters are included which must be adjusted to other vegetation types.

In the scheme the incoming longwave radiation $L^+$ is parameterized with Swinbank's (1963) formula and the cloud-cover correction by Paltridge and Platt (1976). The agreement with our observations is reasonable. An improvement could possibly be obtained by adapting $L^+$ to the nighttime temperature (and humidity) profile in the lowest 100 m.

For the calculation of the outgoing longwave radiation $L^-$, we use Stefan-Boltzmann's law. Here the surface radiation temperature $T_s$ is related to the temperature $T_0$ at the height of the effective roughness length of momentum $z_0$. We have found that, typically, $T_0 - T_s \approx 1$–2 K if $u_* > 0.3$ m s$^{-1}$, but for low wind speeds $T_0 - T_s$ may increase up to 6 K. Based on our observations a parameterization is proposed for $(T_0 - T_s)/\theta_*$ as a function of $u_*$. A discussion is given between the difference in our findings and those of literature (e.g., Garratt and Hicks 1973; Brutsaert 1982). Further verification with independent data, however, is recommended.

The parameterizations of the longwave radiation terms provide the net radiation. Subsequently, the soil heat flux $G$ is parameterized, which is generally an important term in the nighttime energy balance. It appears that a new formulation for $G$ in terms of sensible heat flux and isothermal net radiation is a good descriptor. In our approach we also take account of the influence of water vapor transport in the soil, which is known as distillation or dew rise (Monteith 1963).

The remaining terms in the surface energy budget are the surface fluxes of sensible heat ($H$) and latent heat ($\lambda E$). The latter quantity is described with an equation similar to the usual Penman-Monteith equation (e.g., Monteith 1981). During nighttime this relation shows a balance of two opposite terms, normally resulting in small values of $\lambda E$. For small wind speeds condensation occurs, while for large wind speed evaporation occurs. For the latter case a canopy resistance is used, which is large compared with normal daytime values (e.g., De Bruin and Holtslag 1982).

The model equations and parameterizations of the scheme are used to obtain all components of the surface radiation and energy balance. For very low wind speeds (10 m wind speed $\leq 0.5$ m s$^{-1}$) no turbulence can be maintained in the surface layer. The latter is connected to a critical wind speed, a critical temperature difference and a critical bulk Richardson number of 1.4. Above the critical wind speed the present formulations show good agreement with our observations, on average. Because of the generally low values of the terms in the energy budget, the uncertainty in the data is quite significant. The output of the scheme is illustrated as a function of the main forcing terms.

The surface fluxes of heat and momentum from the present scheme are used to simulate the Cabauw temperature profile up to 80 m in stable conditions. For this purpose we have adopted semiempirical extensions of the log-linear profile (Hicks 1976; Carson and Richards 1977). A new analytical approximation to the latter findings is given. It appears that the Cabauw observations are well-described by the present methods up to $z/L \approx 7$, which is far above the surface layer.

The present model equations can be regarded as extensions of the proposals by Van Ulden and Holtslag (1983, 1985). Also, the empirical aproaches by Venkatram (1980) and Holtslag and Van Ulden (1982) are consistent with the present approach. These approaches were used by Holtslag (1984) for the estimation of stable wind profiles and by Nieuwstadt (1984b) for the calculation of the turbulent boundary layer depth.

Because of its reasonable agreement with observations and its physical basis we believe that the present scheme is relevant for several applications of boundary layer meteorology and related fields. For instance, the equations can be used for stability estimation of the air in pollution dispersion models. Also the present scheme can be used as a surface layer module for short-term weather forecast models, for applications in agricultural meteorology (frost prediction), and in remote sensing studies (e.g., the interpretation of infrared imageries).

*Acknowledgments.* Comments on a draft of this paper by Prof. L. Wartena, Dr. A. P. van Ulden, Mr. H. R. A. Wessels, Dr. A. C. M. Beljaars and the referees are gratefully acknowledged. Discussions with Mr. W. Slob and Dr. H. F. M. ten Berge concerning the soil heat flux were very helpful. The typing was carefully performed by Mrs. Birgit Kok.

## REFERENCES

Beljaars, A. C. M., 1982: The derivation of fluxes from profiles in perturbed areas. *Bound.-Layer Meteor.*, **24**, 35–55.

——, P. Schotanus and F. T. M. Nieuwstadt, 1983: Surface layer similarity under nonuniform fetch conditions. *J. Climate Appl. Meteor.*, **22**, 1800–1810.

Brunt, D., 1932: Notes on radiation in the atmosphere: I. *Quart. J. Roy. Meteor. Soc.*, **58**, 389–420.

Brutsaert, W. H., 1975: On a derivable formula for long-wave radiation from clear skies. *Water Resour. Res.*, **11**, 742–744.

——, 1982: *Evaporation into the atmosphere.* D. Reidel Publishing Company.

Carson, D. J., and P. J. R. Richards, 1978: Modelling surface turbulent fluxes in stable conditions. *Bound.-Layer Meteor.*, **14**, 67–81.

De Bruin, H. A. R., and A. A. M. Holtslag, 1982: A simple parameterization of the surface fluxes of sensible and latent heat during daytime compared with the Penman-Monteith concept. *J. Appl. Meteor.*, **21**, 1610–1621.

Driedonks, A. G. M., H. van Dop and W. M. Kohsieh, 1978: Meteorological observations of the 213 m mast at Cabauu in the Netherlands. *Proceedings of the fourth Symposium on Meteorological Observations and Instrumentation*, Boston, Amer. Meteor. Soc., 41–46.

Dyer, A. J., 1974: A review of flux-profile relationships. *Bound.-Layer Meteor.*, **7**, 363–372.

Estournel, C., and D. Geudalia, 1985: Influence of geostrophic wind on atmospheric nocturnal cooling. *J. Atmos. Sci.*, **42**, 2695–2698.

Garratt, J. R., 1978: Transfer characteristics for a heterogeneous surface of large aerodynamic roughness. *Quart. J. Roy. Meteor. Soc.*, **104**, 491–502.

——, and B. B. Hicks, 1973: Momentum, heat and water vapor transfer to and from natural and artificial surfaces. *Quart. J. Roy. Meteor. Soc.*, **99**, 680–687.

Groen, P., 1947: Note on the theory of noctural radiational cooling of the earth's surface. *J. Meteor.*, **4**, 63–66.

Hicks, B. B., 1976; Wind profile relationships from the "Wangara" experiment. *Quart. J. Roy. Meteor. Soc.*, **102**, 535–551.

——, 1983: A study of dewfall in an acid region: An analysis of Wangara data. *Quart. J. Roy. Meteor. Soc.*, **109**, 900–904.

Holtslag, A. A. M., 1984: Estimates of diabatic wind speed profiles from near surface weather observations. *Bound.-Layer Meteor.*, **29,** 225–250.

——, and A. P. van Ulden, 1982: Simple estimates of nighttime surface fluxes from routine weather data. Scientific Rep. 82–4, Royal Netherlands Meteorological Institute, De Bilt.

——, and ——, 1983: A simple scheme for daytime estimates of the surface fluxes from routine weather data. *J. Climate Appl. Meteor.*, **22,** 517–529.

——, and F. T. M. Nieuwstadt, 1986: Scaling the atmospheric boundary layer. *Bound.-Layer Meteor.*, **36,** 201–209.

Keijman, J. Q., and H. A. R. de Bruin, 1979: A comparison of measured and calculated temperatures of a grass covered surface. *Eos Trans.*, **60**(32), 583.

Kondo, J., O. Kanechika and N. Yasuda, 1978: Heat and momentum transfers under strong stability in the atmospheric surface layer. *J. Atmos. Sci.*, **35,** 1012–1021.

Monin, A. S., and A. M. Yaglom, 1971: *Statistical Fluid Mechanics: mechanics of turbulence. Vol. I.* M.I.T. Press.

Monteith, J. L., 1963: Dew: facts and fallacies, *The Water Relations of Plants,* A. J. Rulter, and F. H. Whitehead, Eds., Blackwell, 37–56.

——, 1981: Evaporation and surface temperature. *Quart. J. Roy. Meteor. Soc.*, **107,** 1–27.

Nieuwstadt, F. T. M., 1978: The computation of the friction velocity $u_*$ and the temperature scale $T_*$ from temperature and wind velocity profiles by least-square methods. *Bound.-Layer Meteor.*, **14,** 235–246.

——, 1984a: The turbulent structure of the stable, nocturnal boundary layer. *J. Atmos. Sci.*, **41,** 2202-2216.

——, 1984b: Some aspects of the turbulent stable boundary layer. *Bound.-Layer Meteor.*, **30,** 31–55.

Obukhov, A. M., 1946: Turbulence in an atmosphere with a non-uniform temperature. *Tr. Akad. Nauk. SSSR Inst. Teorel. Geofis.*, **1** (translation in *Bound.-Layer Meteor* 4–9, **2,** 1971, 7–29.)

Oke, T. R., 1978: *Boundary Layer Climates.* Methuen, 372 pp.

Paltridge, G. W., and C. M. R. Platt, 1976: *Radiative processes in meteorology and climatology. Development in Atm. Science,* **5,** Elseivier, 318 pp.

Priestley, C. H. B., and R. J. Taylor, 1972: On the assessment of surface heat flux and evaporation using large scale parameters. *Mon. Wea. Rev.*, **100,** 81–92.

Slatyer, R. O., and I. C. McIlroy, 1961: *Practical Microclimatology,* CSIRO, 310 pp.

Swinbank, W. C., 1963: Longwave radiation from clear skies. *Quart. J. Roy. Meteor. Soc.*, **89,** 339–348.

——, 1964: Discussion on the 1963 article. *Quart. J. Roy. Meteor. Soc.*, **90,** 488–493.

Ten Berge, H. F. M., 1986: Heat and water transfer at the bare soil surface: Aspects affecting thermal imagery. Ph.D. thesis, Agricultural University of Wageningen, The Netherlands.

Turner, J. S., 1973: *Buoyancy effects in fluids,* Cambridge University Press, 368 pp.

Van Ulden, A. P., and A. A. M. Holtslag, 1983: The stability of the atmospheric surface layer during nighttime. *Sixth Symp. on Turbulence and Diffusion,* Boston, Amer. Meteor. Soc., 257–260.

——, and ——, 1985: Estimation of atmospheric boundary layer parameters for diffusion applications. *J. Climate Appl. Meteor.*, **24,** 1196–1207.

Van Wijk, W. R., and W. J. Derksen, 1963: Sinusoidal temperature variation in a layered soil. *Physics of Plant Environment,* W. R. van Wijk, Ed., North-Holland Publ. Comp, 171–209.

Venkatram, A., 1980: Estimating the Monin-Obukhov Length in the stable boundary layer for dispersion calculations. *Bound.-Layer Meteor.*, **19,** 481–485.

Wessels, H. R. A., 1984: Cabauw meteorological data tapes 1973–1984; description of instrumentation and data processing for the continuous measurements. Scientific Rep. 84–6, Royal Netherlands Meteorological Institute, De Bilt.

Wieringa, J., 1976: An objective exposure correction method for average wind speeds measured at a sheltered location. *Quart. J. Roy. Meteor. Soc.*, **102,** 241–253.